ARL-MR-1002 ● JULY 2019

DEVCOM ARMY RESEARCH LABORATORY

Evaluation of the Bridgman Analysis for Notched Tension Specimens

by Brian M Powers

NOTICES

Disclaimers

The findings in this report are not to be construed as an official Department of the Army position unless so designated by other authorized documents.

Citation of manufacturer's or trade names does not constitute an official endorsement or approval of the use thereof.

Destroy this report when it is no longer needed. Do not return it to the originator.

ARL-MR-1002 ● JULY 2019

Evaluation of the Bridgman Analysis for Notched Tension Specimens

by Brian M Powers
Weapons and Materials Research Directorate, CCDC Army Research Laboratory

REPORT DOCUMENTATION PAGE

Form Approved
OMB No. 0704-0188

1. REPORT DATE *(DD-MM-YYYY)*	2. REPORT TYPE	3. DATES COVERED (From - To)
July 2019	Memorandum Report	August 2018–January 2019

4. TITLE AND SUBTITLE
Evaluation of the Bridgman Analysis for Notched Tension Specimens

5a. CONTRACT NUMBER

5b. GRANT NUMBER

5c. PROGRAM ELEMENT NUMBER

6. AUTHOR(S)
Brian M Powers

5d. PROJECT NUMBER

5e. TASK NUMBER

5f. WORK UNIT NUMBER

7. PERFORMING ORGANIZATION NAME(S) AND ADDRESS(ES)
US Army Research Laboratory
Weapons and Materials Research Directorate (ATTN: FCDD-RLW-MB)
Aberdeen Proving Ground, MD 21005

8. PERFORMING ORGANIZATION REPORT NUMBER
ARL-MR-1002

9. SPONSORING/MONITORING AGENCY NAME(S) AND ADDRESS(ES)

10. SPONSOR/MONITOR'S ACRONYM(S)

11. SPONSOR/MONITOR'S REPORT NUMBER(S)

12. DISTRIBUTION/AVAILABILITY STATEMENT
Approved for public release; distribution is unlimited.

13. SUPPLEMENTARY NOTES

14. ABSTRACT
The Johnson–Cook failure model requires knowledge of the stress state in the test specimen at the moment of failure to fit the model parameters to experimental data. This work compares two methods for determining the stress state in a plastically deformed tension specimen: an analytical solution developed in 1952 by PW Bridgman and a nonlinear finite element solution. The Bridgman solution makes simplifying assumptions about the plastically deformed zone in the specimen to formulate a closed-form solution. Solutions are presented for cylindrical tension specimens and prenotched tensions specimens that are typically used to determine Johnson–Cook failure parameters. Comparisons with finite element results show that Bridgman's assumptions are incorrect, which lead to poor predictions of the stress state in test specimens, and that the finite element results are a more accurate predictor of the stress state.

15. SUBJECT TERMS
Johnson–Cook failure, plasticity, Bridgman analysis, notched tension specimens, stress state

16. SECURITY CLASSIFICATION OF:			17. LIMITATION OF ABSTRACT	18. NUMBER OF PAGES	19a. NAME OF RESPONSIBLE PERSON
a. REPORT	b. ABSTRACT	c. THIS PAGE			Brian M Powers
Unclassified	Unclassified	Unclassified	UU	27	19b. TELEPHONE NUMBER (Include area code) 410-306-1961

Contents

List of Figures

List of Tables

1. Introduction

The failure and damage progression of ductile metals depends on the stress state. Material models that predict failure use some combination of stress invariants to capture the nature of the stress state (e.g., pressure and pure shear). Simple models may only use one measure of stress state while more-complicated models use multiple measures. All of these models require that the stress state is known at the point of failure in a test specimen. Since plastic deformation is nonlinear, the stress state at failure cannot be known a priori. Some type of analysis of the deformed test specimen is needed to determine the stress in the specimen. The Johnson–Cook (JC) failure model is discussed as a common material model used in simulations and an example for why the parameters cannot be fit directly from experimental results. In the past, an analysis developed by Bridgman[1] that requires the geometry of the deformed test specimen has been used to calculate the stress state of test specimens at failure.

The JC strength and failure models[2] are widely used in the computational modeling of high-strain-rate applications. Failure is modeled by having the failure strain depend on stress triaxiality, the strain rate, and homologous temperature, as shown in Eq. 1:

$$\epsilon_f = [D_1 + D_2\, exp(D_3\sigma^*)]\left[1 + D_4\, ln\left(\dot{\epsilon}_{pl}\right)\right][1 + D_5 T^*]. \tag{1}$$

The fracture strain, ϵ_f, is defined as the natural logarithm of ratio of the initial cross-sectional area of the test sample to the cross-sectional area at failure, or

$$\epsilon_f = ln\left(\frac{A_0}{A_f}\right). \tag{2}$$

The homologous temperature is then defined in Eq. 3 as

$$T^* = \frac{T - T_0}{T_m - T_0}. \tag{3}$$

In Eq. 3, T is the current temperature, T_0 is the reference, or initial, temperature, and T_m is melting temperature. The stress triaxiality is defined in Eq. 4 as

$$\sigma^* = \frac{\sigma_m}{\sigma_{eq}}. \tag{4}$$

Here, σ_m is the mean, or hydrostatic, stress and σ_{eq} is the equivalent, or von Mises stress.

Determining the constants in Eq. 1 involves performing mechanical tests until failure at different triaxialities, strain rates, and temperatures. The area at failure is then measured and used to calculate the failure strain using Eq. 2. Fitting the

mechanical test data for the temperature and strain rate are fairly straightforward. Generating the data for the stress triaxiality is more complicated. Different test-specimen geometries are needed to create different stress triaxialities. Common types of specimen geometry used are the notched tension specimens.[3] These geometries are cylindrical tension specimens with notches of various radii machined into the gage length. A schematic of the notched specimens is shown in Fig. 1 and the radii of the notches are presented in Table 1. The cross-sectional areas in both the notched and unnotched regions are constant among the different notch radii. After testing, a stress analysis, either analytical or computational, is done to determine the triaxiality.

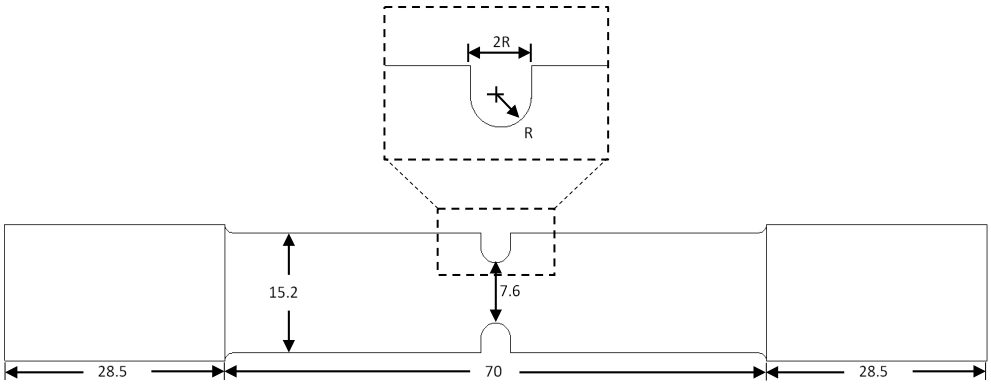

Fig. 1 Geometry of the notched tension specimens from Mackenzie et al.[3]

Table 1 Notch dimensions for the notched tension specimens in Fig. 1

Specimen	R (mm)
A	3.8
B	2.54
C	1.90
D	1.27
E	6.34

More complex failure models[4,5] have been developed that account for not just the stress triaxiality but also the Lode angle. These failure theories account for more-complex stress states that can affect the failure behavior of ductile materials. The Lode coordinates are a set of cylindrical coordinates defined in the principal stress space. They can be thought of as a set of r, θ, z coordinates that depend on the stress state, specifically the stress invariants, and are defined as

$$r = \sqrt{2J_2}\,, \tag{5}$$

$$z = \frac{I_1}{\sqrt{3}}\,, \tag{6}$$

and

$$sin(3\theta_s) = cos(3\theta_c) = \frac{J_3}{2}\left(\frac{3}{J_2}\right)^{\frac{3}{2}}\,. \tag{7}$$

In Eqs. 5–7, J_2 and J_3 are the second and third invariants of the deviatoric stress tensor while I_1 is the first invariant of the full stress tensor. In the current work, we will define a Lode parameter, L, as

$$L = sin(3\,\theta_s)\,. \tag{8}$$

An analytical stress analysis often used for the notched tension specimens is one developed by Bridgman,[1] who based the assumptions on observations from numerous experimental tests. The Bridgman analysis predicts the stresses developed in the necked region of a cylindrical tension specimen.

In the current work, finite-element (FE) models were used to determine the stress states in cylindrical and notched tension specimens. The FE results of the cylindrical specimen are used to check the assumptions Bridgman used in developing the analysis. The notched-tension FE results are subsequently used to determine if the Bridgman analysis is valid for notched tension specimens.

2. Summary of the Bridgman Analysis

A major assumption of the Bridgman analysis is that the plastic strain does not vary through the thickness of the necked region. Bridgman justified this assumption from careful observation of numerous experimental tests. The stress state in the necked region of a cylindrical tension specimen based on Bridgman's analysis is

$$\sigma_r = -P + F\,ln\left(\frac{a^2+2aR-r^2}{2aR}\right), \tag{9}$$

$$\sigma_\theta = -P + F\,ln\left(\frac{a^2+2aR-r^2}{2aR}\right), \tag{10}$$

and

$$\sigma_z = -P + F + F\,ln\left(\frac{a^2+2aR-r^2}{2aR}\right). \tag{11}$$

In Eqs. 9–11, P is the externally applied pressure, a is the radius measured from the centerline in the necked region, R is the radius of the circle that osculates the deformed profile in the necked region, and r is the radial coordinate measured from the centerline. For all cases considered in this report, $P = 0$. Bridgman terms F the "flow stress" at the outer boundary of the necked region. It is equivalent to the σ_z stress at a where $\sigma_r = \sigma_\theta = 0$, and is defined as

$$F = \frac{Load}{\pi a^2 \left(1+\frac{2R}{a}\right) ln\left(1+\frac{a}{2R}\right)} . \quad (12)$$

The parameters a and R must be experimentally measured during deformation. Mackenzie et al.,[3] used the Bridgman analysis for determining the stresses in notched tension specimens even though the analysis was not developed for initially notched geometries. In calculating the stresses for the notched specimens, a and R parameters are assumed to be the initial geometric parameters of the notched specimens.

3. Numerical Analysis

3.1 Cylindrical Tension Specimen

An FE simulation of a cylindrical test specimen was created and analyzed using the ABAQUS[6] FE commercial software package. The geometry has the same dimensions as the notched specimens detailed in Mackenzie et al.,[3] but without the notch. The axisymmetric FE geometry comprised half of the gage length of specimens, ignoring the threaded portion of the specimen, and were discretized with approximately 8000 axisymmetric, linear, reduced-integration CAX4R elements. The geometry radius is 7.2 mm and modeled length is 35 mm. Figure 2 shows a schematic of the FE model with the boundary conditions. Symmetry boundary conditions (BCs) were used along the bottom edge and the centerline. A z direction displacement BC was placed at the top edge to provide the tensile loading, while the r direction displacements were fixed on the same edge. The clamped BC along the top edge is often assumed to be a valid representation for the tensile test specimens.

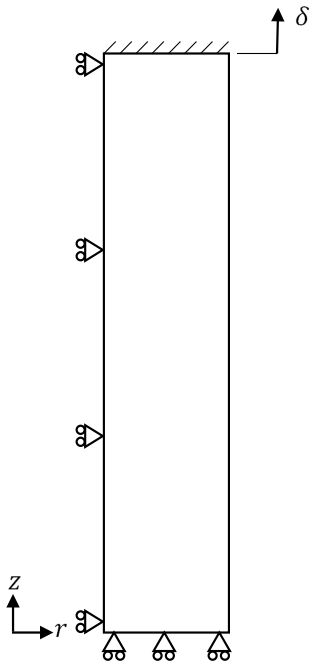

Fig. 2 Schematic of the boundary conditions applied on the FE model: Symmetry boundary conditions are applied at $r = 0$ and $z = 0$; r direction displacement is fixed at $z = 35$; load is applied through z direction displacement at $z = 3$.

An elastic-perfectly plastic material model is used with properties that approximate A36[7] structural steel. The three material properties required for the material model are Young's modulus, Poisson ratio, and yield strength; respectively, $E = 250\ GPa$, $\nu = 0.27$, and $\sigma_y = 250\ MPa$.

3.2 Notched Tension Specimens

FE simulations analyzed the notched-tension-specimen geometries from Mackenzie et al.,[3] which are reproduced in Fig. 1. The boundary conditions, material properties, and number and type of elements are identical to the cylindrical specimens. There are five different notch radii, R, presented in Mackenzie et al., who labeled them A–E. The notch radii, R, are shown in Table 1. In the order of descending notch radii, the specimen labels are E, A, B, C, and D; so, E is the largest notch and D the smallest.

4. Results and Discussion

4.1 Cylindrical Tension Specimen

The Bridgman analysis requires determination of the deformed geometric parameters a and R. The values for a are the specimen radius of the necked region at the $y = 0$ plane. To determine R from the FE mesh, the position of the outer edge of the sample in the necked region is needed. The positions of the five closest nodes to the $y = 0$ plane were taken from the results. A least-squares method was used to fit the nodal positions to a circle[8] to determine the radius R. To achieve a better fit and to guarantee the center of the circle is on the $y = 0$ plane, the nodal position data was mirrored; that is, $u_x(x, -y) = u_x(x, y)$, $u_y(x, -y) = -u_y(x, y)$. Once a and R are determined, Eqs. 9–11 are used to determine the Bridgman stress state.

Figure 3 shows the plastic strain, ϵ_z^{pl}, in the necked region at increasing levels of deformation. Initially, the plastic strain is uniform across the cross-section, but as the deformation increases, the plastic strain becomes increasingly nonuniform.

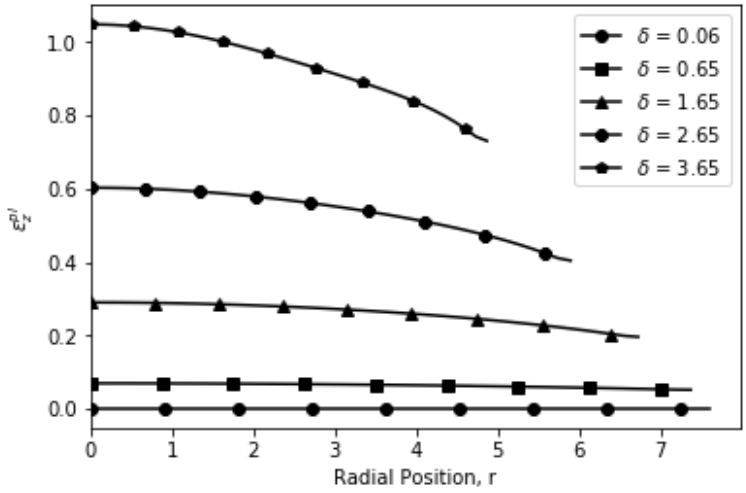

Fig. 3 Plastic strain, ϵ_z^{pl}, in the necked region

Figures 4–6 compare the direct stresses, $\sigma_r, \sigma_\theta, \sigma_z$, obtained from the FE analysis with the stresses calculated with the Bridgman equations. Two displacement levels are shown.

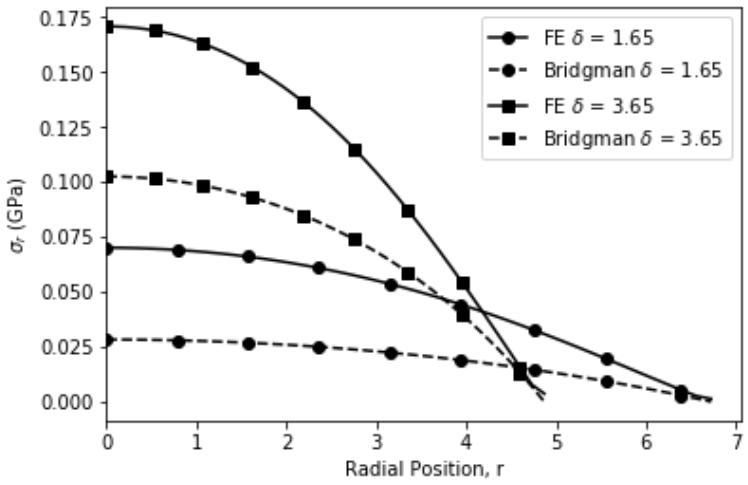

Fig. 4 Comparison of the r-direction stress in the necked region for the cylindrical tension specimen

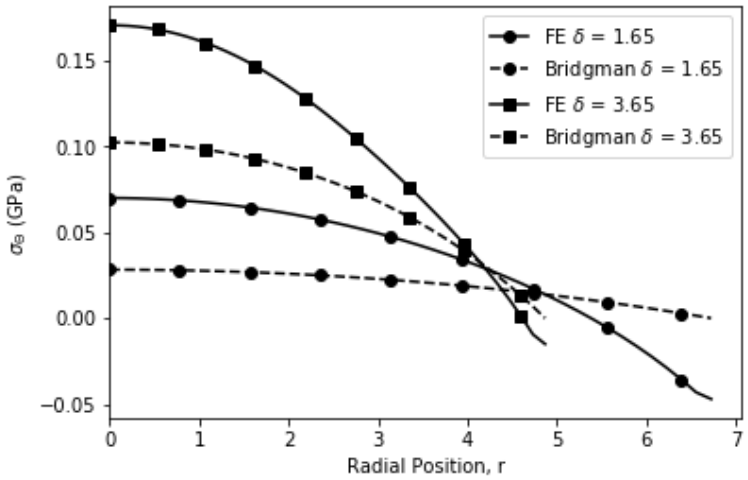

Fig. 5 Comparison of the θ-direction stress in the necked region for the cylindrical tension specimen

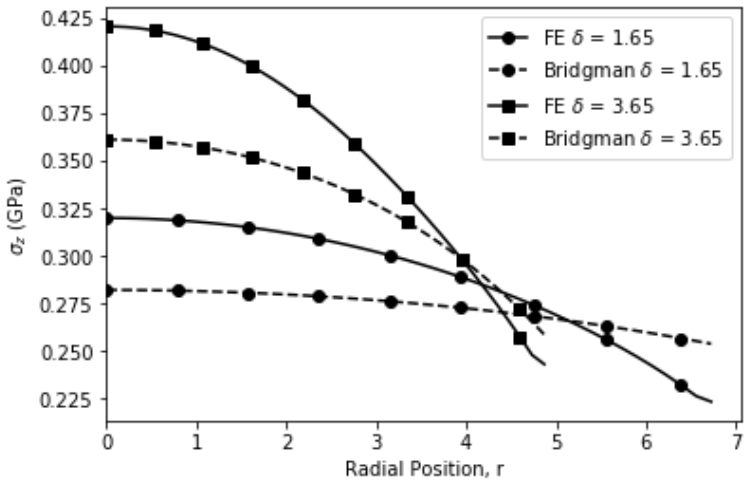

Fig. 6 Comparison of the z-direction stress in the necked region for the cylindrical tension specimen

Figures 7–9 show a comparison of the equivalent stress, σ_{eq}, triaxiality, and Lode parameter at the same displacements.

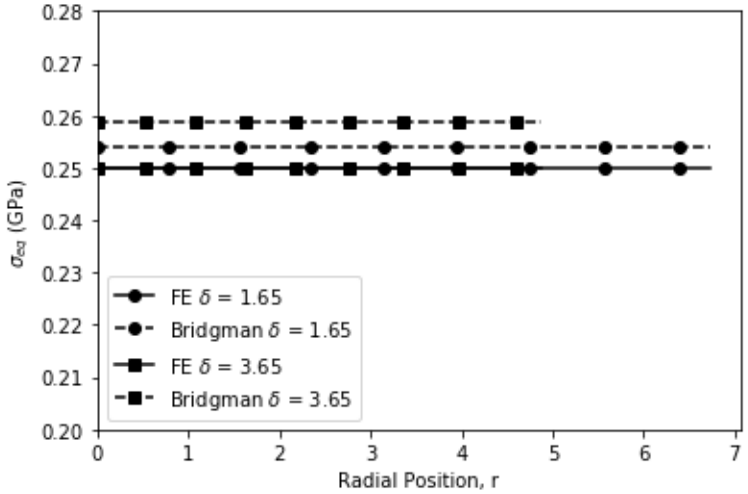

Fig. 7 Comparison of the equivalent stress in the necked region for the cylindrical tension specimen

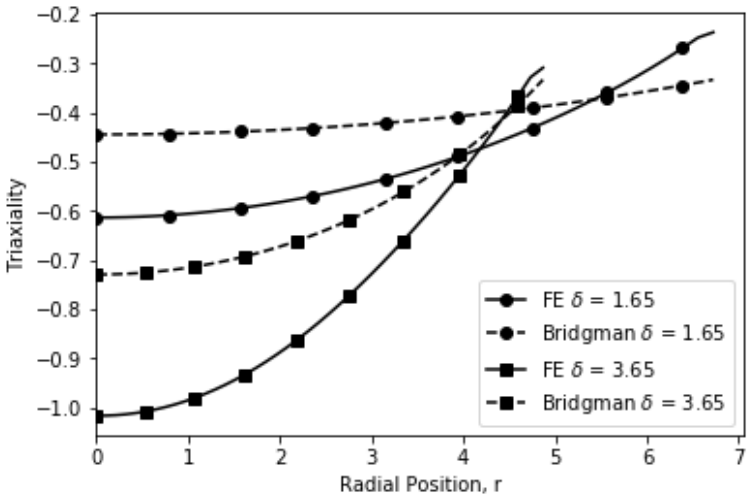

Fig. 8 Comparison of the triaxiality in the necked region for the cylindrical tension specimen

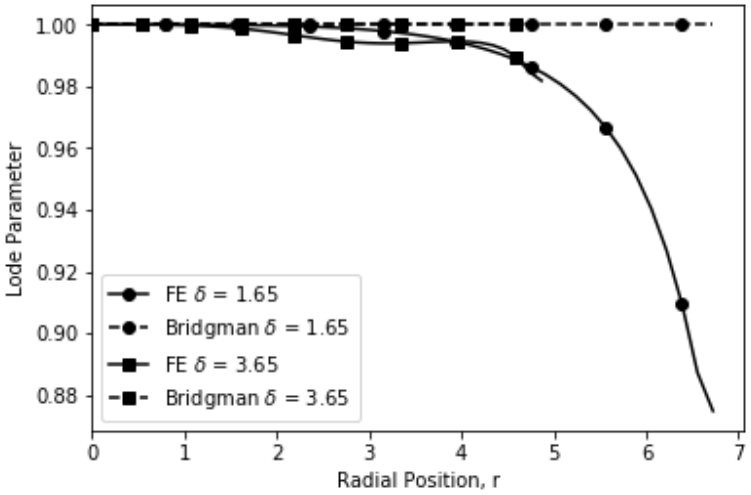

Fig. 9 Comparison of the Lode parameter in the necked region for the cylindrical tension specimen

The Bridgman analysis underpredicts the maximum stress in all cases. The equivalent stress is in quite-good agreement, within 4%. In developing the analysis, Bridgman assumed that ϵ_z is constant across the necked cross-section. This, along with a requirement of incompressibility for plastic deformation, led to $\epsilon_r = \epsilon_\theta$. From inspection Bridgman knew that a stress solution where $\sigma_r = \sigma_\theta$ would satisfy this last requirement. This is not the only possible stress state to satisfy $\epsilon_r = \epsilon_\theta$, but it was used by Bridgman. The FE results in Figs. 4 and 5 show that $\sigma_r \neq \sigma_\theta$. At the outer edge, $\sigma_r = 0$, which is required for a traction-free surface, but σ_θ is not. The equivalent stress, σ_{eq}, does match, but that is because, in a sense, the analysis

is designed to capture it. Bridgman defined the parameter F as the "flow stress" at $r = a$ in the necked region. During plastic deformation, the flow stress is equal to the equivalent stress. In fact, substituting Eqs. 9–11 into the definition of equivalent stress leads to $\sigma_{eq} = F$. These plots clearly show that the triaxiality does not match between the Bridgman and FE cases. The Lode parameter matches close to the center of the specimen, but this is expected. The Lode parameter is a measure of ratio of direct stress to shear stress. Since the centerline of the specimen has no shear stresses (due to symmetry requirements), the Lode parameter is always 1 at this location.

4.2 Notched Tension Specimens

The plastic strain in the z-direction, ε_z^{pl}, is shown in Fig. 10 as function of radial position in the notched region for increasing displacements, δ. For small displacements, ε_z^{pl} is fairly uniform through the notched region but as the displacement increases, there is significant variation in ε_z^{pl}. The quality of the deformed mesh was checked to ensure the results were not invalid because of overly deformed elements. The quality of the mesh was still good for each of the cases at the maximum reported deformations. The mesh for Notch D is shown in Fig. 11 at $\delta = 0.087$ as a typical example.

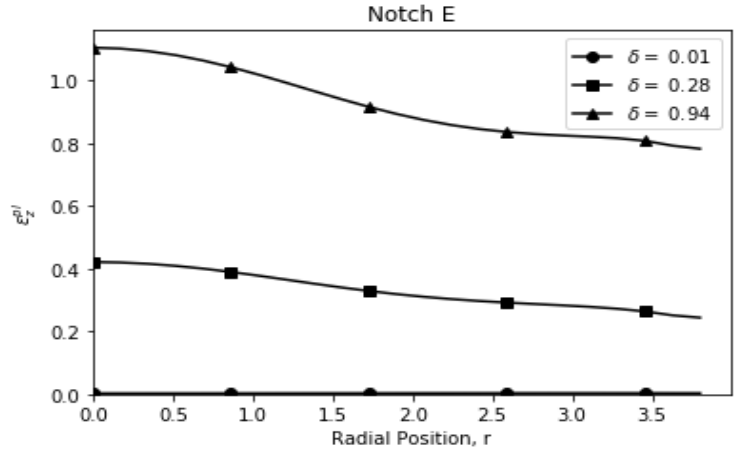

(a)

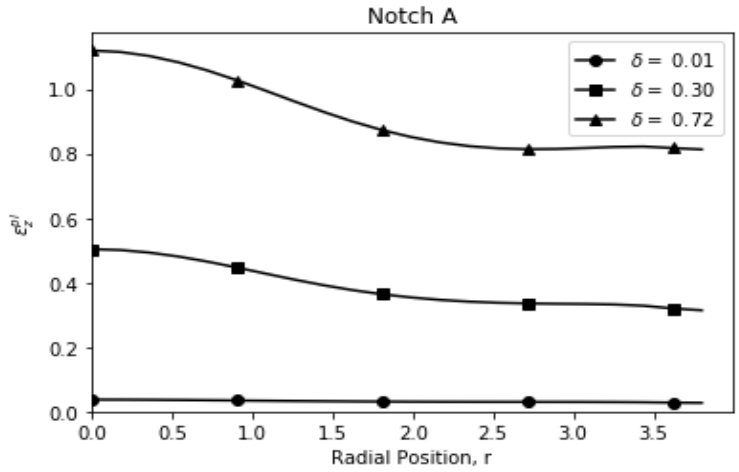

(b)

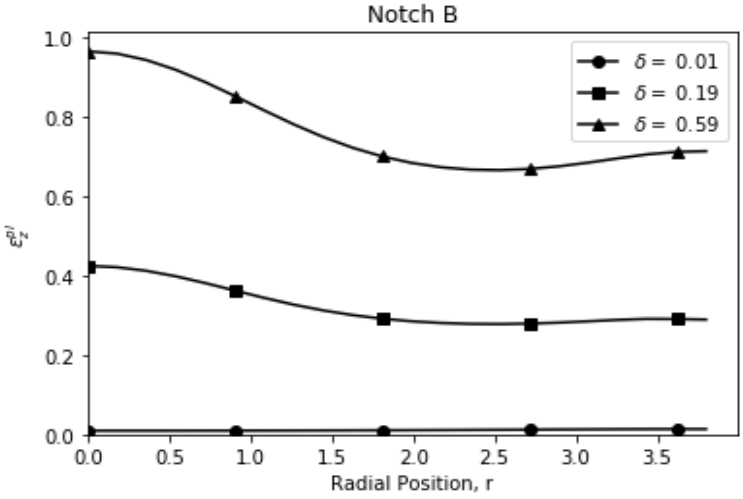

(c)

Fig. 10 Axial (z-direction) plastic strain, ϵ_z^{pl}, through the cross-section of the notched region

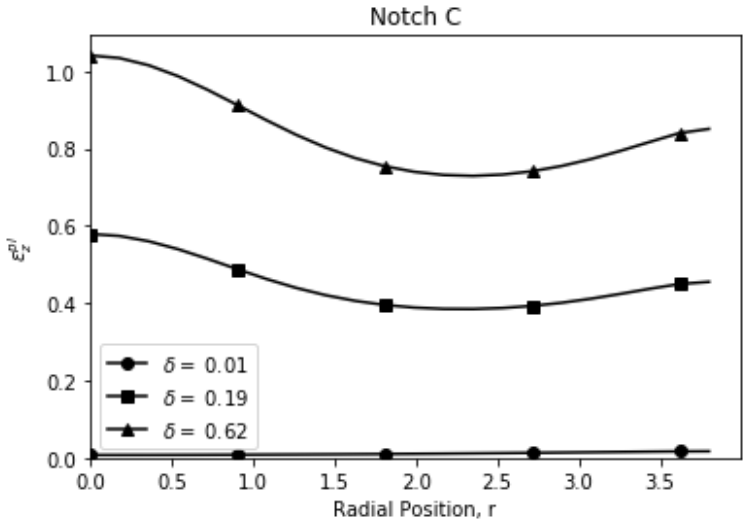

(d)

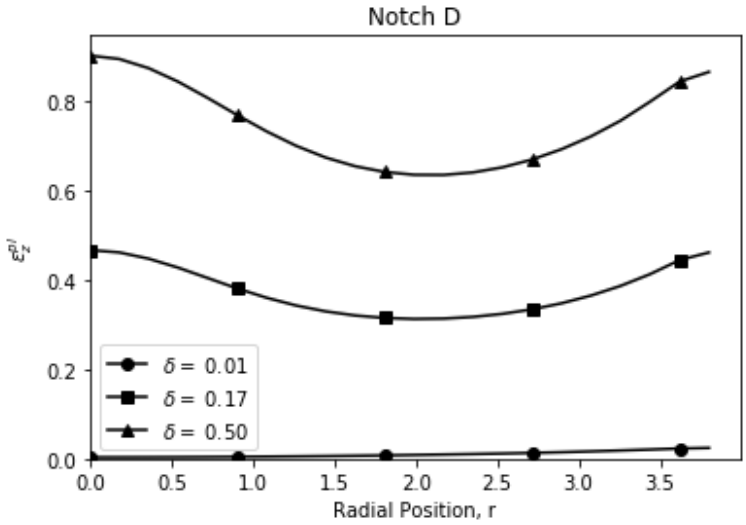

(e)

Fig. 10 Axial (z-direction) plastic strain, ϵ_z^{pl}, through the cross-section of the notched region (continued)

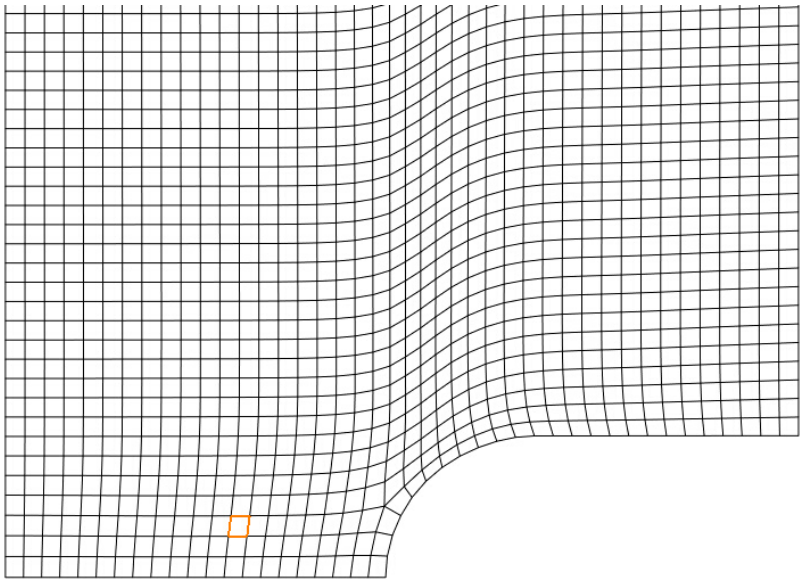

Fig. 11 Deformed mesh around the notch for Specimen D at $\delta = 0.087$

A comparison between the Bridgman analysis and the FE results of the stress in the z-direction are shown in Fig. 12. There is significant error in the Bridgman analysis compared to the FE results. A consequence of using only the initial a and R values is that the F parameter does not depend on deformed geometry and only changes proportionally with the applied load. Comparisons of r and θ directions, while not shown, also exhibit high levels of disagreement.

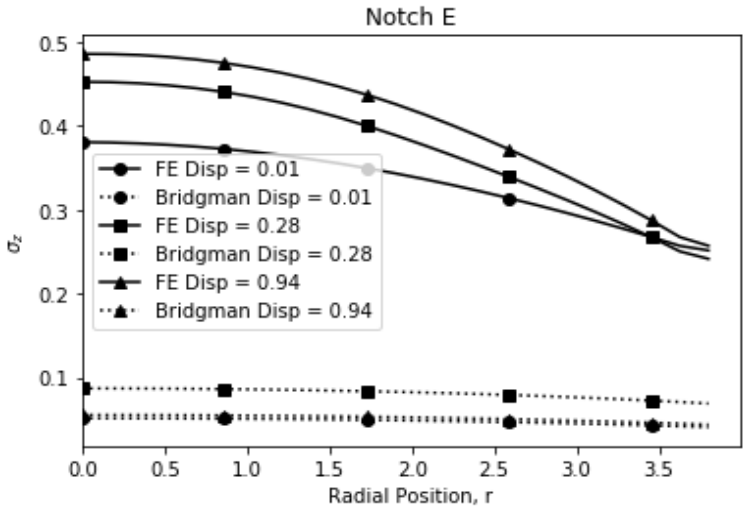

(a)

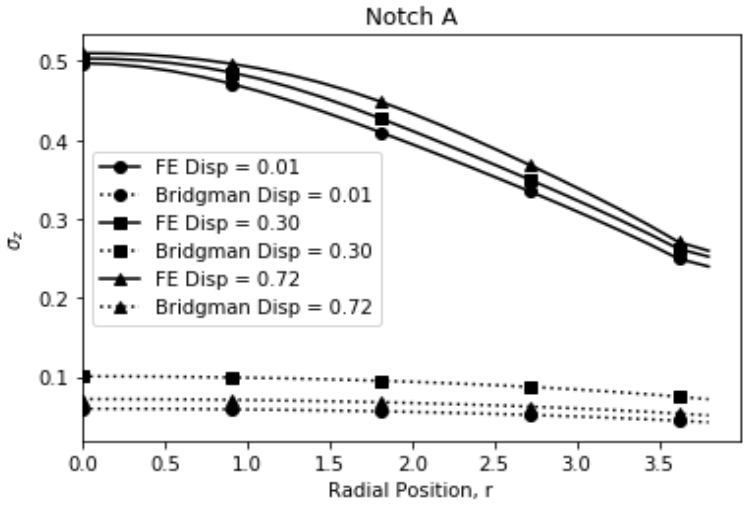

(b)

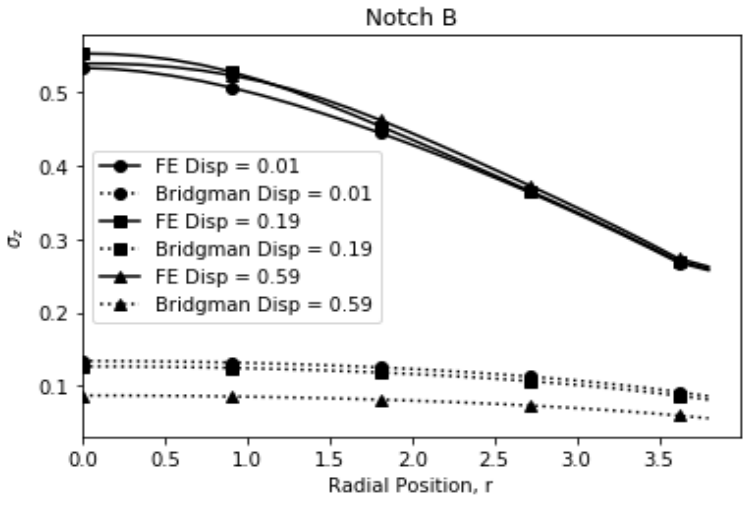

(c)

Fig. 12 Axial (z-direction) stress, σ_z, through the cross-section of the notched region for each notch

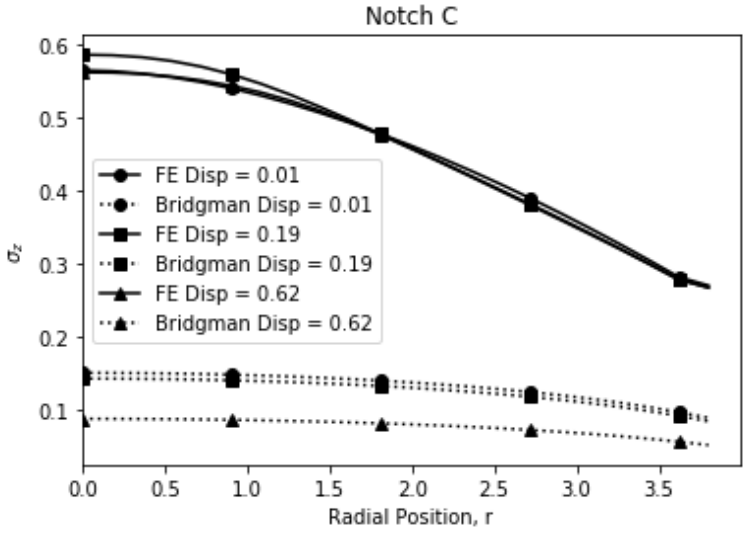

(d)

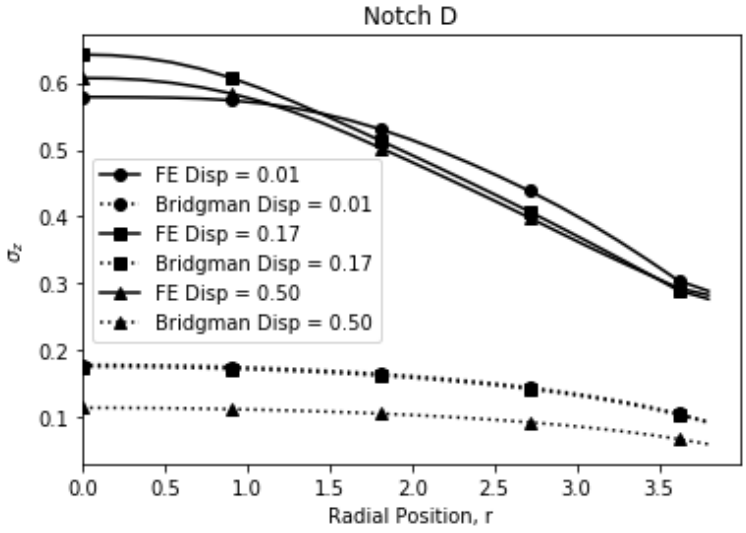

(e)

Fig. 12 Axial (z-direction) stress, σ_z, through the cross-section of the notched region for each notch (continued)

A comparison of the equivalent stress is shown in Fig. 13. Unlike for the cylindrical specimen, the Bridgman analysis does not match the FE results for the equivalent stress.

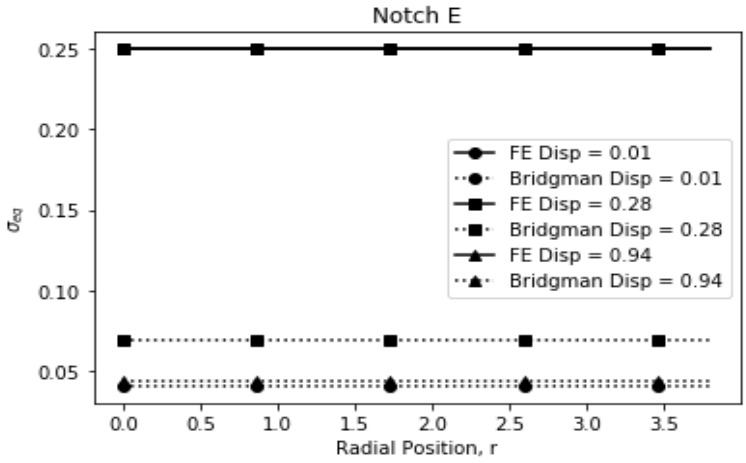

(a)

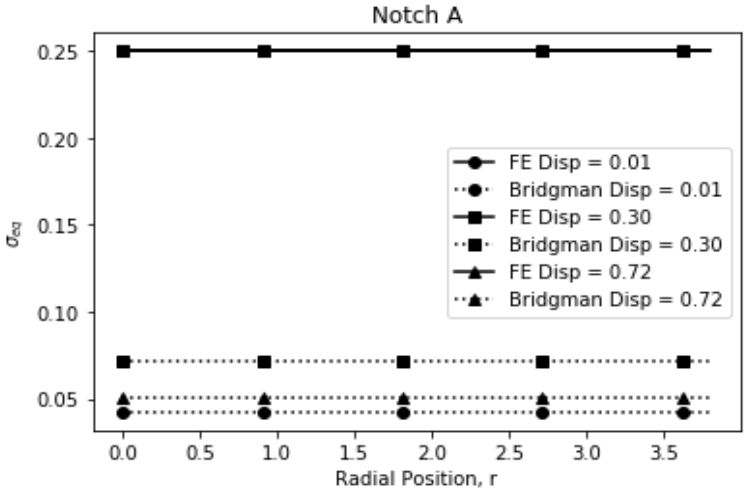

(b)

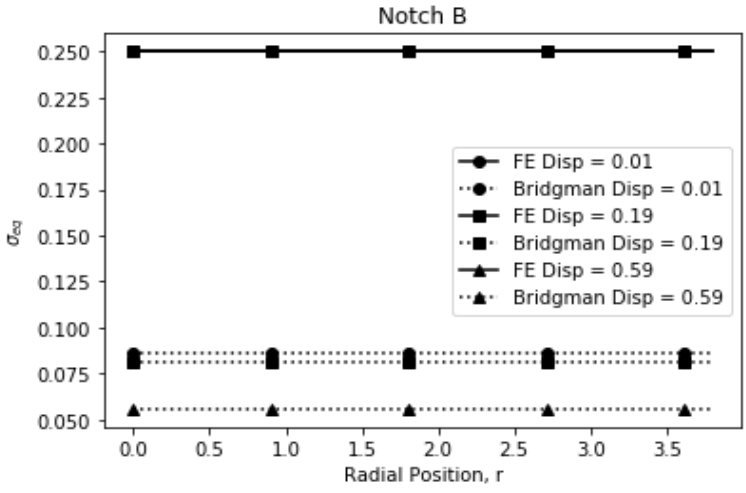

(c)

Fig. 13 Equivalent stress, σ_{eq}, through the cross-section of the notched region for each notch

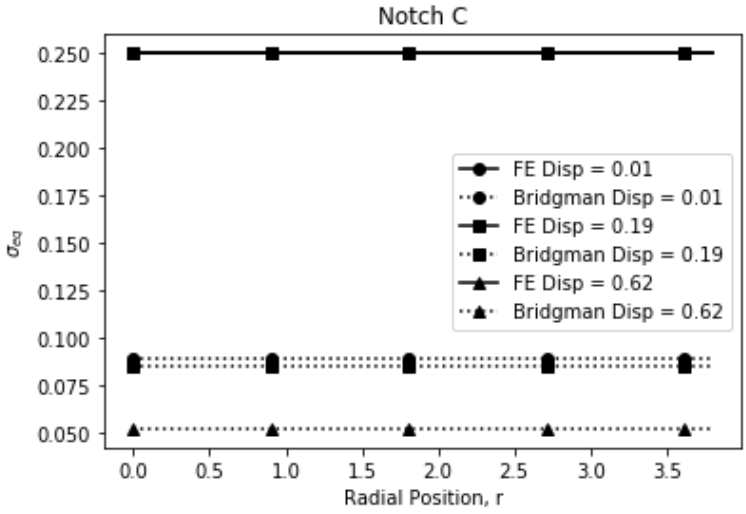

(d)

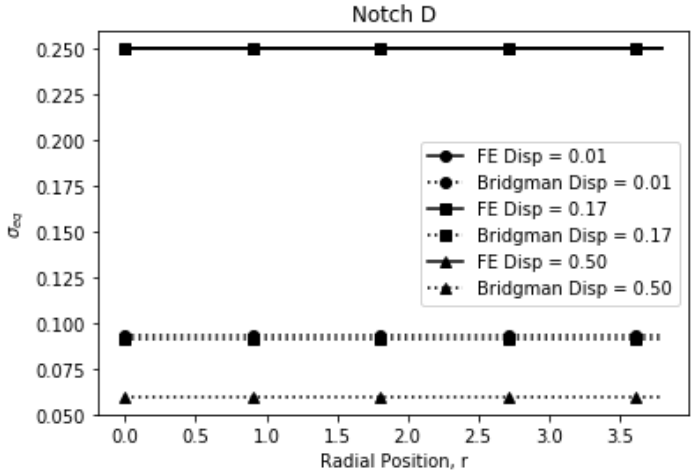

(e)

Fig. 13 Equivalent stress, σ_{eq}, through the cross-section of the notched region for each notch (continued)

5. Conclusions

The results of finite-element simulations of a cylindrical tension specimen and notched tension specimens are compared to the analytical Bridgman analysis. The Bridgman analysis assumes the plastic strain, ϵ_z^{pl}, is constant through the necked region and that $\sigma_r = \sigma_\theta$. For the cylindrical tension specimen, the FE results show that both of those assumptions are invalid. The equivalent stress, σ_{eq}, is in good agreement between the FE results and the Bridgman analysis, but the individual stress components and the triaxiality are not. The Lode parameter shows good agreement between the two approaches at the center of the specimen, $r = 0$, but the results diverge at the outer edge of the sample. The agreement at $r = 0$ is

because the center of the specimen has no shear in either analysis, and when no shear stress is present, the Lode parameter, L, is 1.

For the notched tension specimens, using the undeformed values of a and R as Mackenzie et al.,[3] leads to poor comparisons between the FE results and the Bridgman analysis, including the equivalent stress, σ_{eq}. Comparisons of the triaxiality and Lode parameter were not made since the other stress components showed significant disagreement. Using updated deformed values for a and R, from techniques like digital-image correlation, might improve the agreement between the two analysis approaches. Since the Bridgman analysis was not developed for notched specimens and the FE results show the assumptions for cylindrical specimens are invalid, using updated a and R values is not expected to improve the Bridgman results sufficiently for use in evaluating notched tension specimens.

The Bridgman analysis was originally developed for materials that continually harden. The elastic-perfectly plastic material model violates this hardening assumption. Since it was initially developed, the Bridgman analysis has been applied to materials such as ductile metals to determine the stress state at failure, even though such materials typically stop hardening close to failure, thus violating this assumption for the validity of Bridgman analysis. Further work that investigates other plastic flow rules (e.g., linear or power law) needs to be done to determine how the hardening rule affects the accuracy of the Bridgman analysis.

6. References

1. Bridgman PW. Studies in large plastic flow and fracture: with special emphasis on the effects of hydrostatic pressure. New York (NY): McGraw-Hill; 1952.
2. Johnson GR, Cook WH. Fracture characteristics of three metals subjected to various strains, strain rates, temperatures and pressures. Eng Frac Mech. 1985;21(1):31–48.
3. Mackenzie AC, Hancock JW, Brown DK. On the influence of state of stress on ductile failure initiation in high strength steels. Eng Frac Mech. 1977;9(1):167–188.
4. Alves Ml, Jones N. Influence of hydrostatic stress on failure of axisymmetric notched specimens. J Mech Phys Solids. 1999;47(3):643–667.
5. Malcher L, Mamiya EN. An improved damage evolution law based on continuum damage mechanics and its dependence on both stress triaxiality and the third invariant. Int J Plasticity. 2014;56:232–261.
6. Systèmes D. ABAQUS 6.14 user's manual. Providence (RI): Dassault Systèmes; 2014.
7. Gere JM, Timoshenko S. Mechanics of materials. 3rd ed. Boston (MA): PWS-Kent Publishing Company; 1990. p. xviii, 807.
8. Least squares circle. SciPy Cookbook; 2011 [accessed 2018 Jun 15]. https://scipy-cookbook.readthedocs.io/items/Least_Squares_Circle.html.

List of Symbols, Abbreviations, and Acronyms

BC	boundary condition
FE	finite element
JC	Johnson–Cook

1 (PDF)	DEFENSE TECHNICAL INFORMATION CTR DTIC OCA
1 (PDF)	GOVT PRINTG OFC A MALHOTRA
2 (PDF)	DIR CCDC ARL IMAL HRA RECORDS MGMT RDRL DCL TECH LIB
1 (PDF)	CCDC ARL FCDD RLW MB B M POWERS